Transient Climate Response in a Two-Layer Energy-Balance Model. Part II: Representation of the Efficacy of Deep-Ocean Heat Uptake and Validation for CMIP5 AOGCMs

O. GEOFFROY, D. SAINT-MARTIN, G. BELLON, AND A. VOLDOIRE

Centre National de Recherches Météorologiques, Groupe d'études de l'Atmosphère Météorologique (CNRM-GAME), Toulouse, France

D. J. L. OLIVIÉ

Center for International Climate and Environmental Research–Oslo, and University of Oslo, Oslo, Norway

S. TYTÉCA

Centre National de Recherches Météorologiques, Groupe d'études de l'Atmosphère Météorologique (CNRM-GAME), Toulouse, France

(Manuscript received 11 April 2012, in final form 28 August 2012)

ABSTRACT

In this second part of a series of two articles analyzing the global thermal properties of atmosphere–ocean coupled general circulation models (AOGCMs) within the framework of a two-layer energy-balance model (EBM), the role of the efficacy of deep-ocean heat uptake is investigated. Taking into account such an efficacy factor is shown to amount to representing the effect of deep-ocean heat uptake on the local strength of the radiative feedback in the transient regime. It involves an additional term in the formulation of the radiative imbalance at the top of the atmosphere (TOA), which explains the nonlinearity between radiative imbalance and the mean surface temperature observed in some AOGCMs. An analytical solution of this system is given and this simple linear EBM is calibrated for the set of 16 AOGCMs of phase 5 of the Coupled Model Intercomparison Project (CMIP5) studied in Part I. It is shown that both the net radiative fluxes at TOA and the global surface temperature transient response are well represented by the simple EBM over the available period of simulations. Differences between this two-layer EBM and the previous version without an efficacy factor are analyzed and relationships between parameters are discussed. The simple model calibration applied to AOGCMs constitutes a new method for estimating their respective equilibrium climate sensitivity and adjusted radiative forcing amplitude from short-term step-forcing simulations and more generally a method to compute their global thermal properties.

1. Introduction

In Part I (Geoffroy et al. 2013, hereafter Part I), it is shown using the database from phase 5 of the Coupled Model Intercomparison Project (CMIP5) that a two-layer energy-balance model calibrated only from one atmosphere–ocean coupled general circulation model (AOGCM) step-forcing experiment is able to reproduce the idealized scenario with gradual CO_2 increase. Such a calibration gives the first-order global thermal properties characterizing an AOGCM. The calibration method requires the determination of both the reference radiative forcing amplitude and the equilibrium climate sensitivity (ECS), defined as the equilibrium mean surface temperature response for a $2\times CO_2$ radiative perturbation.

Determining the ECS and the amplitude of the radiative forcing associated with a given externally imposed perturbation remains an issue and a topic of debate in the literature (e.g., Knutti and Hegerl 2008). While the evaluation of the radiative forcing is complicated by the existence of fast stratospheric and tropospheric adjustments (Gregory and Webb 2008), the determination of

Corresponding author address: Olivier Geoffroy, Centre National de Recherches Météorologiques (CNRM-GAME) 42 av. G. Coriolis, 31057 Toulouse, France.
E-mail: olivier.geoffroy@meteo.fr

DOI: 10.1175/JCLI-D-12-00196.1

© 2013 American Meteorological Society

the ECS of a given AOGCM requires very long simulations (thousands of years) and is computationally expensive. Alternative methods have been proposed for estimating the equilibrium climate sensitivity. For example, it can be evaluated by coupling the atmospheric general circulation model to a mixed-layer ocean (AGCM-ML). However, an AOGCM and its AGCM-ML counterparts' estimates of the ECS may differ because the ocean impacts the earth's energy balance. On the one hand, the ocean circulation redistributes energy. On the other hand, some components such as the sea ice or the cloud field may react differently according to the representation of the ocean (Williams et al. 2008).

Another type of method consists of extrapolating the transient regime AOGCM's response to equilibrium. These methods lie on the linear assumption between the top-of-the-atmosphere (TOA) radiative imbalance N and the mean surface temperature T response $N = \mathcal{F} - \lambda T$, where $\mathcal{F}$ is the adjusted radiative forcing and λ is the feedback parameter. Murphy (1995) introduced the effective climate sensitivity such that it can be deduced from the unbalanced mean surface temperature response and the amplitude of the radiative imbalance $\mathrm{ECS}/T(t) = \mathcal{F}_{2\times\mathrm{CO}_2}/[\mathcal{F}_{2\times\mathrm{CO}_2} - N(t)]$. But this estimation requires the knowledge of the radiative forcing $\mathcal{F}_{2\times\mathrm{CO}_2}$, which must be deduced by an independent method. Gregory et al. (2004) refined the estimate of the effective ECS by fitting the net radiative flux at TOA as a function of T during the whole period of an abrupt $2\times\mathrm{CO}_2$ or a stabilization scenario. This introduces the concept of effective forcing. Such a fit gives the effective forcing (intercept), the effective radiative feedback parameter (slope), and the effective equilibrium climate sensitivity (x axis intersection). The estimated forcing takes into account all the fast (few months) feedbacks that cannot be considered as feedbacks associated with the surface temperature response, such as stratospheric and tropospheric adjustments (Gregory and Webb 2008).

The main shortcoming of this type of method is that the ECS is found to vary in time for some models and methods (Gregory et al. 2004; Senior and Mitchell 2000; Boer and Yu 2003b). This questions the validity of the linear assumption between the radiative response of the climate system and T that is at the heart of energy-balance models (EBMs). Williams et al. (2008) showed that a bias in the estimation of the radiative forcing is partly responsible for these variations but not totally; the assumption of linearity itself has limitations. Indeed, whereas the assumption of linear dependence between the radiative response and T is reasonably robust in equilibrium, it is found not to be valid during the transient regime for some climate models (Gregory et al. 2004; Williams et al. 2008; Winton et al. 2010; Andrews et al. 2012).

Using CMIP3 idealized scenario simulations, Winton et al. (2010) showed that an additional process needs to be taken into account during the transient regime in order to represent the evolution of the radiative imbalance of the climate system. The ocean heat uptake reduces the rate of warming and this effect occurs preferentially in some regions, especially those corresponding to the sinking branches of the thermohaline circulation, in the North Atlantic ocean and the circumpolar ocean of the Southern Hemisphere (Manabe et al. 1991). This modifies the transient regime temperature pattern in comparison with the equilibrium pattern. Because the feedback strength varies geographically, the pattern of surface temperature change induced by the ocean heat uptake may impact the radiative imbalance in the transient regime. This reasoning led Winton et al. (2010) to introduce an efficacy factor for the ocean heat uptake. Held et al. (2010) introduced such an efficacy factor in the two-layer linear EBM.

In this study, this simple model is used to determine the ECS, the adjusted radiative forcing, and the thermal inertia properties of a given AOGCM by taking into account the effect of deep-ocean heat uptake on the radiative imbalance during the transient regime. This allows consistent computation of all the parameters in a single framework. In section 2, the model with this feature is presented, underlying assumptions of the model are discussed, and the calibration method is described. In section 3, this method is applied to CMIP5 abrupt $4\times\mathrm{CO}_2$ experiments. Results are discussed and compared with those obtained from the previous version of the EBM, without the efficacy factor. The existence of relationships between the parameters is then investigated. Finally, a decomposition of the TOA net radiative flux in longwave and shortwave components is performed within the framework of this simple model.

2. Two-layer model with an efficacy factor for deep-ocean heat uptake

a. System of equations and analytical solution

In this part, we consider the following two-layer EBM with an efficacy factor for deep-ocean heat uptake ε proposed by Held et al. (2010):

$$C\frac{dT}{dt} = \mathcal{F} - \lambda T - \varepsilon\gamma(T - T_0) \quad \text{and} \tag{1}$$

$$C_0\frac{dT_0}{dt} = \gamma(T - T_0), \tag{2}$$

where C, C_0, and γ are the first-layer (atmosphere/land/upper ocean) heat capacity, the second-layer (deep

ocean) heat capacity (both expressed per unit area), and the heat-exchange coefficient between the two layers, respectively. The term $\gamma(T - T_0)$ is the heat flux H exchanged between the two layers and is equal to the deep-ocean heat uptake $H = \gamma(T - T_0)$. Since the change in the heat content of the first layer $C(dT/dt)$ is driven by the sum of the heat flux exchanged with the deep ocean $-H$ and the heat flux exchanged with the external system N, the net radiative flux at TOA evolves as

$$N = \mathcal{F} - \lambda T - (\varepsilon - 1)H. \tag{3}$$

In the following, EBM-1 will refer to the standard energy-balance model analyzed in Part I and EBM-ε to the model described above. The presence of an additional radiative flux term, $-(\varepsilon - 1)H$, in the evolution of N constitutes the difference with the EBM-1.

By introducing $C_0' = \varepsilon C_0$ and $\gamma' = \varepsilon\gamma$, the system can be written as follows:

$$C\frac{dT}{dt} = \mathcal{F} - \lambda T - \gamma'(T - T_0) \quad \text{and} \tag{4}$$

$$C_0'\frac{dT_0}{dt} = \gamma'(T - T_0), \tag{5}$$

which is the same mathematical system as that of the EBM-1 except for the primes. As pointed out by Held et al. (2010), the effect of the deep-ocean efficacy factor is equivalent to modifying ocean properties such that the deep-ocean heat capacity and the heat-exchange coefficient between the two layers are scaled by a factor ε. Note that EBM-ε is physically different from the EBM-1 because it includes one additional process. As a result, all the physical parameters estimated on the basis of this model can be different from their counterparts estimated within the framework of EBM-1. The derivation of the analytical solution of EBM-ε is straightforward. All the formulations of the mode parameters given in Part I are still valid by replacing C_0 and γ with C_0' and γ', respectively. These parameters are noted with the primes in the following. The mean surface temperature response for a step forcing is

$$T(t) = \frac{\mathcal{F}}{\lambda} - \frac{\mathcal{F}}{\lambda}a_f' e^{-t/\tau_f'} - \frac{\mathcal{F}}{\lambda}a_s' e^{-t/\tau_s'} \tag{6}$$

and for a linear forcing with an increase rate k is

$$T(t) = \frac{k}{\lambda}t - \frac{k}{\lambda}\tau_f' a_f'(1 - e^{-t/\tau_f'}) - \frac{k}{\lambda}\tau_s' a_s'(1 - e^{-t/\tau_s'}), \tag{7}$$

where τ_f', a_f', τ_s', and a_s' are the fast and slow mode parameters defined in Part I and expressed as functions of λ, C, C_0', and γ'.

b. EBM-ε underlying hypothesis

1) GLOBAL BUDGET

In this section, the hypotheses underlying the introduction of an efficacy factor ε are presented. Within the framework of a two-layer simple climate model, the change in the heat content of the climate system is the sum of the atmosphere/land/upper-ocean instantaneous heat uptake $C(dT/dt)$ and the deep-ocean instantaneous heat uptake $C_0(dT_0/dt)$. This change is equal to the net radiative imbalance at the top of the climate system N,

$$C\frac{dT}{dt} + C_0\frac{dT_0}{dt} = N. \tag{8}$$

The net radiative imbalance N is the sum of the radiative forcing and of the radiative response R_T of the climate system induced by the surface air temperature change

$$N = \mathcal{F} + R_T. \tag{9}$$

Thus, the radiative response R_T can be decomposed as the sum of three radiative responses, an equilibrium radiative response $R_{\text{eq}} = -\mathcal{F}$ and the radiative responses R_U and R_D equal to the instantaneous rate of heat storage in the upper and the deep oceans, respectively. Similarly to the forcing that constitutes a source of heat (in the case of a positive radiative forcing) for the first layer, the ocean heat uptake constitutes a sink of heat and is associated with a surface temperature change. The equilibrium radiative response can be expressed as a linear function of the equilibrium temperature response. Analogously, we introduce the temperature changes T_U and T_D associated with the upper-ocean and the deep-ocean heat uptake, respectively, such that R_U and R_D are linear functions of T_U with a feedback parameter λ and of T_D with a feedback parameter λ_D, respectively. This leads to the following system of equations:

$$-\mathcal{F} = R_{\text{eq}} = -\lambda T_{\text{eq}}, \tag{10}$$

$$C\frac{dT}{dt} = R_U = -\lambda T_U, \quad \text{and} \tag{11}$$

$$C_0\frac{dT_0}{dt} = H = R_D = -\lambda_D T_D. \tag{12}$$

The deep-ocean heat-uptake temperature is associated with a different feedback parameter λ_D because the spatial pattern of T_D differs from the equilibrium temperature response pattern. This point is discussed in more detail in the next section.

By assuming additivity of the temperature response patterns (Forster et al. 2000; Boer and Yu 2003a), the

surface air temperature response is the sum of the three balance responses,

$$T = T_{\rm eq} + T_U + T_D. \tag{13}$$

The sum $T_U + T_D$ is the disequilibrium temperature difference associated with the deep-ocean heat uptake $T_H = T - T_{\rm eq}$ (Winton et al. 2010; Part I). The sum of the radiative responses associated with T_U and T_D is equal to the radiative imbalance, $R_U + R_D = N$.

Summing Eqs. (10)–(12) gives the first layer energy budget,

$$C\frac{dT}{dt} + H = \mathcal{F} - \lambda T_{\rm eq} - \lambda T_U - \lambda_D T_D. \tag{14}$$

By using the decomposition of T [Eq. (13)], Eq. (14) leads to

$$C\frac{dT}{dt} + H = \mathcal{F} - \lambda T - (\lambda - \lambda_D)T_D. \tag{15}$$

Following Hansen et al. (2005), Held et al. (2010), and Winton et al. (2010), an efficacy factor ε for deep-ocean heat uptake is introduced,

$$\varepsilon = \lambda/\lambda_D. \tag{16}$$

By using this definition and $T_D = -H/\lambda_D$, Eq. (15) is equivalent to Eq. (1).

In the case of a gradual increase of the external perturbation, $C(dT/dt)$ is small (see section 3c in Part I); in the limit of negligible $C(dT/dt)$, $N = H$ and Eq. (3) leads to the formulation of Winton et al. (2010) [see their Eq. (3)]

$$T_{\rm eq} - T = \frac{\varepsilon}{\lambda}N, \tag{17}$$

with the equilibrium temperature response defined as $T_{\rm eq} = \mathcal{F}/\lambda$.

2) LOCAL BUDGET

To understand why the feedback strength may vary with the temperature pattern, it can be useful to examine the evolution of the local energy balance in transient regime. As pointed out by Boer and Yu (2003a), the change in heat content of a climate system column is equal to the local radiative imbalance and the local convergence of the horizontal energy

$$\frac{dh^i}{dt} + \frac{dh_0^i}{dt} = \mathcal{F}^i - \lambda^i T^i + A_t^i + A_{0t}^i, \tag{18}$$

where dh^i/dt and dh_0^i/dt are the local change in the heat content of the first and the second layer, respectively; T^i, $\mathcal{F}^i$, and λ^i are the local temperature response, the local forcing, and the local feedback parameter; respectively; and A_t^i and A_{0t}^i are the local convergence of the horizontal energy flux of the first and the second layer, respectively. The superscript i denotes local values. The average over the earth's surface of dh^i/dt or dh_0^i/dt is the change in the heat content of the first layer $C(dT/dt)$ or of the second layer $C_0(dT_0/dt)$, respectively. The global mean of the local forcing is $\mathcal{F}$. The global average of each local energy convergence A_t^i and A_{0t}^i is 0. Note that the local heat flux from the upper ocean to the deep ocean H^i satisfies

$$\frac{dh_0^i}{dt} = H^i + A_{0t}^i. \tag{19}$$

Equation (18) can be viewed as the heat budget in response to the sum of three "forcings": the external forcing $\mathcal{F}^i$, and two sink terms, $-dh^i/dt$ and $-dh_0^i/dt$, considered "internal forcings." By assuming additivity of the temperature response patterns, the local surface temperature response is expressed as the sum of the three balance responses, $T^i = T_{\rm eq}^i + T_U^i + T_D^i$, and the local budget (18) can be decomposed in the following system of equations:

$$\mathcal{F}^i - \lambda^i T_{\rm eq}^i + A_{\rm eq}^i + A_{0\rm eq}^i = 0, \tag{20}$$

$$-\frac{dh^i}{dt} - \lambda^i T_U^i + A_U^i + A_{0U}^i = 0, \quad \text{and} \tag{21}$$

$$-\frac{dh_0^i}{dt} - \lambda^i T_D^i + A_D^i + A_{0D}^i = 0, \tag{22}$$

where T_U^i and T_D^i are the local temperature perturbations associated with the upper-ocean and the deep-ocean heat uptake. Here, $A_{\rm eq}^i$, A_U^i, and A_D^i, are the associated convergences of horizontal energy fluxes in the first layer, with $A_t^i = A_{\rm eq}^i + A_U^i + A_D^i$. Similarly, $A_{0\rm eq}^i$, A_{0U}^i, and A_{0D}^i are the convergences of horizontal energy fluxes in the second layer. Note that the global average of each energy-flux convergence A_x^i and A_{0x}^i is zero. Assuming that A_{0U}^i is 0 leads to $A_{0D}^i = A_{0t}^i - A_{0\rm eq}^i$. Also, the decomposition of T and A_t in sums, Eqs. (18) and (20)–(22), leaves 1 degree of freedom in the definition of T_U^i, T_D^i, A_U^i, and A_D^i.

Introducing the normalized equilibrium temperature amplitude function $r_{\rm eq}^i = T_{\rm eq}^i/T_{\rm eq}$, the local heat budget at equilibrium is

$$\mathcal{F}^i - \lambda^i r_{\rm eq}^i T_{\rm eq} + A_{\rm eq}^i + A_{0\rm eq}^i = 0. \tag{23}$$

One can note that the equilibrium temperature pattern (i.e., $r_{\rm eq}^i$) depends on the local forcing, the local

feedback, and the amplitude of the local energy convergence. Thus, the total feedback parameter λ is the average of the local feedback parameter weighted by the equilibrium temperature pattern,

$$\lambda = \frac{1}{S}\int\int r^i_{\rm eq}\lambda^i\, ds, \tag{24}$$

where ds is the surface area element and S is the world surface area. The parameter λ will be referred as the equilibrium feedback parameter in the following.

By assuming the separability of time and space variables for T^i_U and T^i_D, they can be decomposed into the product of a time-varying global average T_x by a spatial pattern r^i_x. The initial conditions in the case of a step forcing impose $T_U(0) = -T_{\rm eq}(0)$ and $T^i_U(0) = -T^i_{\rm eq}(0)$. As a result T_U and $T_{\rm eq}$ have the same pattern, $r^i_U = r^i_{\rm eq}$. Note that the initial conditions of a step-forcing case [$T_U(0) = -T_{\rm eq}(0)$ and $R_U(0) = -R_{\rm eq}(0)$] also directly impose that the feedback parameter associated with T_U in Eq. (11) is the equilibrium feedback parameter. Because the pattern of the deep-ocean heat uptake is different from the pattern of the radiative forcing, T^i_D is assumed to be associated with a pattern, $r^i_D \neq r^i_{\rm eq}$. Averaging Eq. (22) over the earth's surface leads to Eq. (12) with the following formulation of λ_D:

$$\lambda_D = \frac{1}{S}\int\int r^i_D\lambda^i\, ds. \tag{25}$$

The weight coefficient r^i_D is different from the one in the equilibrium feedback parameter expression. If the strength of the local feedbacks is large (which corresponds to low values of λ^i) in regions where the ocean heat uptake induces a small temperature increasing rate (resulting in high values of r^i_D), then λ_D is lower than λ. Consequently, for a given amplitude of T_U and T_D, R_D is smaller (i.e., the climate system accumulates less heat). Note that the assumption of separability of T^i_U and T^i_D in space and time is not necessary. However, in the case when r^i_D is time dependent, another assumption is required to obtain a constant λ_D in Eq. (25).

To conclude section 2b, the introduction of an efficacy factor for the deep-ocean heat uptake $\varepsilon = \lambda/\lambda_D$ is the result of a decomposition of the temperature pattern as the sum of the temperature response patterns to the radiative forcing, the upper-ocean and the deep-ocean heat uptakes assuming a linear relationship between these forcings and their associated temperature responses. Because the spatial pattern of the temperature response to the deep-ocean heat uptake differs from the equilibrium pattern, the spatial heterogeneity of the radiative feedbacks strength implies that the magnitude of the global radiative feedback varies in time during a climate transition.

c. *Effect of efficacy factor of deep-ocean heat uptake*

In case of a step forcing, the analytical solutions for the upper-ocean and deep-ocean heat-uptake temperatures are

$$T_U(t) = -\frac{\mathcal{F}}{\lambda}(f'_U a'_f e^{-t/\tau'_f} + s'_U a'_s e^{-t/\tau'_s}) \quad \text{and} \tag{26}$$

$$T_D(t) = -\frac{\mathcal{F}}{\lambda}(f'_D a'_f e^{-t/\tau'_f} + s'_D a'_s e^{-t/\tau'_s}). \tag{27}$$

The expression, the order of magnitude, and the sign of the fractional contributions a'_f, a'_s, f'_U, f'_D, s'_U, and s'_D are given in Part I (by replacing C_0 and γ with C'_0 and γ' in the expressions, respectively).

The theoretical temporal evolutions of T, T_U, and T_D in the case of a step forcing are represented at the top of Fig. 1 for three values of efficacy factor: $\varepsilon < 1$, $\varepsilon = 1$, and $\varepsilon > 1$, with other parameters unchanged. The upper-ocean heat-uptake temperature T_U increases with the characteristic time scale τ'_f, and after a few years it tends to zero since the contribution s'_U of the slow mode to T_U is negligible, the upper-ocean reservoir is saturated. Concerning the deep-ocean heat-uptake temperature, the contributions of the slow and fast modes (s'_D and f'_D) are comparable but of opposite signs. The fast mode is predominant in the first few years and induces a decrease in T_D; that is, the heat flux exchanged between the two layers H increases because T increases faster than T_0. After this first phase (with a characteristic duration of τ'_f), the slow mode becomes dominant and T_D increases slowly back to zero because the deep ocean accumulates less and less heat.

The middle panels of Fig. 1 represent the theoretical relationship between the radiative imbalance N and the mean surface temperature perturbation T during the transient regime, for the same values of ε. The intercept and the x axis intersection are independent from the value of ε. Per definition, the intercept at $T = 0$ is the amplitude of the forcing $\mathcal{F}$ (Gregory et al. 2004). Similarly, the x axis intersection is the equilibrium temperature response (the equilibrium climate sensitivity in the case of a $2\times CO_2$ perturbation per definition). Only the path to join these two points is altered when ε is modified.

With $\varepsilon = 1$, the net radiative flux varies linearly with the temperature. For $\varepsilon \neq 1$, the plots suggest that there are two distinct stages in the (N, T) response to an abrupt forcing. To understand this behavior, it is convenient to decompose the net flux into the sum of its two components contribution R_U and R_D. In Fig. 1 (middle),

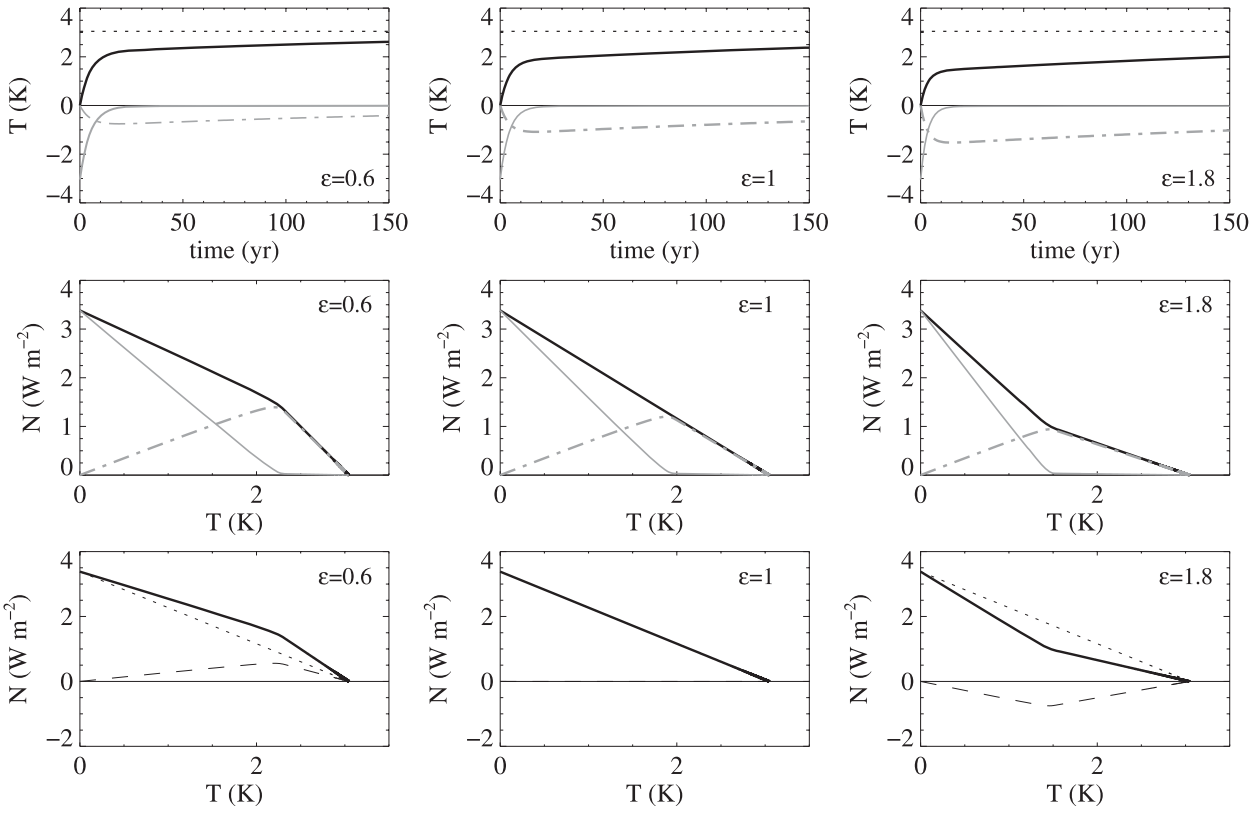

FIG. 1. EBM-ε results. (top) Time evolution of global mean surface air temperature response (thick black line), upper-ocean heat-uptake temperature response T_U (thick gray line), and deep-ocean heat-uptake temperature response T_D (dot-dashed gray line) for a step-forcing case; the black dotted line shows the equilibrium temperature response $T_{\rm eq}$. (middle) Global mean net radiative flux change (thick black line) and its decomposition into $R_U = -\lambda T_U$ (thick gray line) and $R_D = -\lambda_D T_D$ (dot-dashed gray line) as functions of the global mean surface air temperature response. (bottom) Global mean net radiative flux change (thick black line; same as above) and its decomposition into the linear term $\mathcal{F} - \lambda T$ (dotted gray line) and the deviation term $-(\varepsilon - 1)H$ (dashed gray line). Plots are for the three values of ε indicated on the panels and $\mathcal{F} = 3.9$ W m^{-2}, $\lambda = 1.3$ W m^{-2} K^{-1}, $C = 8$ W yr m^{-2} K^{-1}, $C_0 = 100$ W yr m^{-2} K^{-1}, and $\gamma = 0.7$ W m^{-2} K^{-1}.

the evolutions of (R_U, T) and (R_D, T) are plotted respectively with gray solid lines and gray dash-dotted lines.

During the first period, corresponding to the fast mode response time scale, the two components (upper and deep oceans) contribute with similar amplitude but with opposite trends to the temperature response and N varies roughly linearly with T. Indeed, neglecting the slow response term during this period, the time evolutions of R_U and R_D are proportional to that of T_H (and T); the scale factors are $-\lambda f'_U$ and $-\lambda_D f'_D$, with $f'_U > 0$ and $f'_D < 0$, respectively. Accordingly, the radiative imbalance N as the sum of these two contributions evolves roughly linearly with T.

During the second period, the contribution of the upper ocean is negligible ($s'_U \ll 1$) and the net radiative flux is simply the contribution of the deep-ocean heat-uptake temperature, $-\lambda_D T_D$. Then, since $T_D \approx T - T_{\rm eq}$, the radiative flux varies also roughly linearly with T. The sharp change in the trend of the (N, T) line corresponds to a time similar to the fast relaxation time. This analysis suggests that linear fits of the two asymptotes of the (N, T) curve performed separately as in Gregory et al. (2004) give a good approximation of the radiative forcing $\mathcal{F}$ (as the intercept of the first fit), the equilibrium temperature $T_{\rm eq}$ (as the x-axis intersection of the second fit), and $\lambda_D = \lambda/\varepsilon$ (as the slope of the second fit).

The net radiative flux at the top of the atmosphere can also be decomposed as the sum of prognostic variables and physical parameters of the EBM-ε as shown in Eq. (3). The radiative imbalance N is the sum of a linear term $\mathcal{F} - \lambda T$ and a fraction $1 - \varepsilon$ of the instantaneous rate of heat storage in the deep ocean H. Their evolution in the (N, T) space is illustrated in Fig. 1 (bottom). The linear term takes into account the fact that the surface temperature is not in equilibrium, which induces a radiative imbalance. The second term is a deviation from this linear radiative flux due to the nonlinear evolution

of the temperature pattern. The magnitude of H reflects the magnitude of this deviation.

Initially, $H = 0$, $T = 0$, and the radiative imbalance is equal to the forcing. In equilibrium, as H is zero, the assumption of linear dependence between the radiative imbalance and the surface temperature remains valid. But during the transient regime, the net radiative flux is affected by the deep-ocean heat uptake. The parameter usually referred to as the effective feedback parameter $\lambda_{\text{eff}} = (\mathcal{F} - N)/T$ varies in time (if $\varepsilon \neq 1$) and needs to be distinguished from the equilibrium feedback parameter λ. It is equal to the transient radiative feedback factor λ_t, such that

$$\lambda_t = \lambda + (\varepsilon - 1)\gamma\frac{T - T_0}{T}. \tag{28}$$

The efficacy factor can be determined from gradual perturbation AOGCMs simulations [by neglecting $C(dt/dt)$] but requires prior knowledge of the equilibrium climate sensitivity and feedback parameter (Winton et al. 2010). On the other hand, all the EBM-ε radiative and thermal inertia parameters can be consistently computed from only a step-forcing AOGCM experiment (and a control simulation), by taking into account the time evolution of the transient radiative feedback factor. In the next section, the method used to calibrate the EBM-ε physical parameters to a given AOGCM is briefly described.

d. Method for EBM-ε parameter calibration

In comparison with the EBM-1, the EBM-ε has an additional radiative parameter ε that needs to be tuned consistently with the reference radiative forcing amplitude (e.g., $\mathcal{F}_{2\times CO_2}$ for a $2\times CO_2$ perturbation) and the equilibrium feedback parameter λ from the N–T evolution. The physical parameters of the EBM-ε are computed iteratively using a step-forcing experiment. The parameters are initially set to the EBM-1 values ($\varepsilon = 1$, and parameters computed in Part I). For each iteration i, the deep-ocean heat uptake $H^{(i-1)}$ is first evaluated using the analytical solutions and the thermal parameters computed at iteration $(i - 1)$. Then, using Eq. (3), a multilinear regression of N (AOGCM values) against the AOGCM surface temperature response T and $H^{(i-1)}$ provides the values of $\mathcal{F}^{(i)}$, $\lambda^{(i)}$, and $\varepsilon^{(i)}$,

$$N = \mathcal{F}^{(i)} - \lambda^{(i)}T - [\varepsilon^{(i)} - 1]H^{(i-1)}. \tag{29}$$

Finally the thermal inertia parameters $C^{(i)}$, $C_0^{\prime(i)}$ and $\gamma^{\prime(i)}$ are tuned by performing two fits of the surface temperature response following the methodology used for the EBM-1 calibration (see details in section 3 of Part I).

TABLE 1. The $4\times CO_2$ radiative forcing $\mathcal{F}_{4\times CO_2}$, total feedback parameter λ, efficacy factor for deep-ocean heat uptake ε, and $4\times CO_2$ equilibrium temperature $T_{4\times CO_2}$ estimates in the framework of the EBM-ε of the 16 CMIP5 models used in this paper, and their multimodel mean and standard deviation.

Model	$\mathcal{F}_{4\times CO_2}$ (W m^{-2})	λ (W m^{-2} K^{-1})	ε	$T_{4\times CO_2}$ (K)
BCC-CSM1–1	7.4	1.28	1.27	5.8
BNU-ESM	7.3	0.92	0.98	7.9
CanESM2	8.2	1.06	1.28	7.8
CCSM4	8.5	1.4	1.36	6.0
CNRM-CM5.1	7.1	1.12	0.92	6.4
CSIRO-Mk3.6.0	7.0	0.68	1.82	10.2
FGOALS-s2	8.0	0.87	1.21	9.1
GFDL-ESM2M	7.1	1.38	1.21	5.1
GISS-E2-R	9.1	2.03	1.44	4.5
HadGEM2-ES	6.8	0.61	1.54	11.1
INM-CM4	6.0	1.56	0.83	3.9
IPSL-CM5A-LR	6.7	0.79	1.14	8.5
MIROC5	8.9	1.58	1.19	5.6
MPI-ESM-LR	9.4	1.21	1.42	7.8
MRI-CGCM3	7.1	1.31	1.25	5.4
NorESM1-M	7.4	1.15	1.57	6.5
Multimodel mean	7.6	1.18	1.28	7.0
Standard deviation	1.0	0.37	0.25	2.1

Only a few iterations are found to be sufficient to obtain convergence. This method for estimating the equilibrium climate sensitivity, radiative parameters, and thermal inertia parameters from a short-term step-forcing simulation will be referred to in the following as the EBM-ε method. In the next section, the EBM-ε method is applied to 16 CMIP5 AOGCMs using the abrupt $4\times CO_2$ experiments and results are compared with the EBM-1 estimates [which, for the radiative properties, correspond to the estimates from Gregory et al. (2004)'s method].

3. Validation for CMIP5 AOGCMs

a. Radiative parameters and TOA net flux: Comparison with the EBM-1

For the same 16 AOGCMs of the CMIP5 database analyzed in Part I (see Table 4 in Part I for model expansions), the EBM-ε method is applied and radiative parameter values are reported in Table 1. The values of the deep-ocean heat-uptake efficacy factor are mostly greater than 1 (see also Fig. 3a). Excluding the BNU-ESM model that has a value of ε very close to 1, only two models (INM-CM4 and CNRM-CM5.1) have values of ε smaller than unity. The heat-uptake efficacy factor ranges from 0.83 to 1.82 with a multimodel mean value of 1.28 and an intermodel standard deviation of 0.25. These results are in very good agreement with the estimates of Winton et al. (2010) for some CMIP2 and

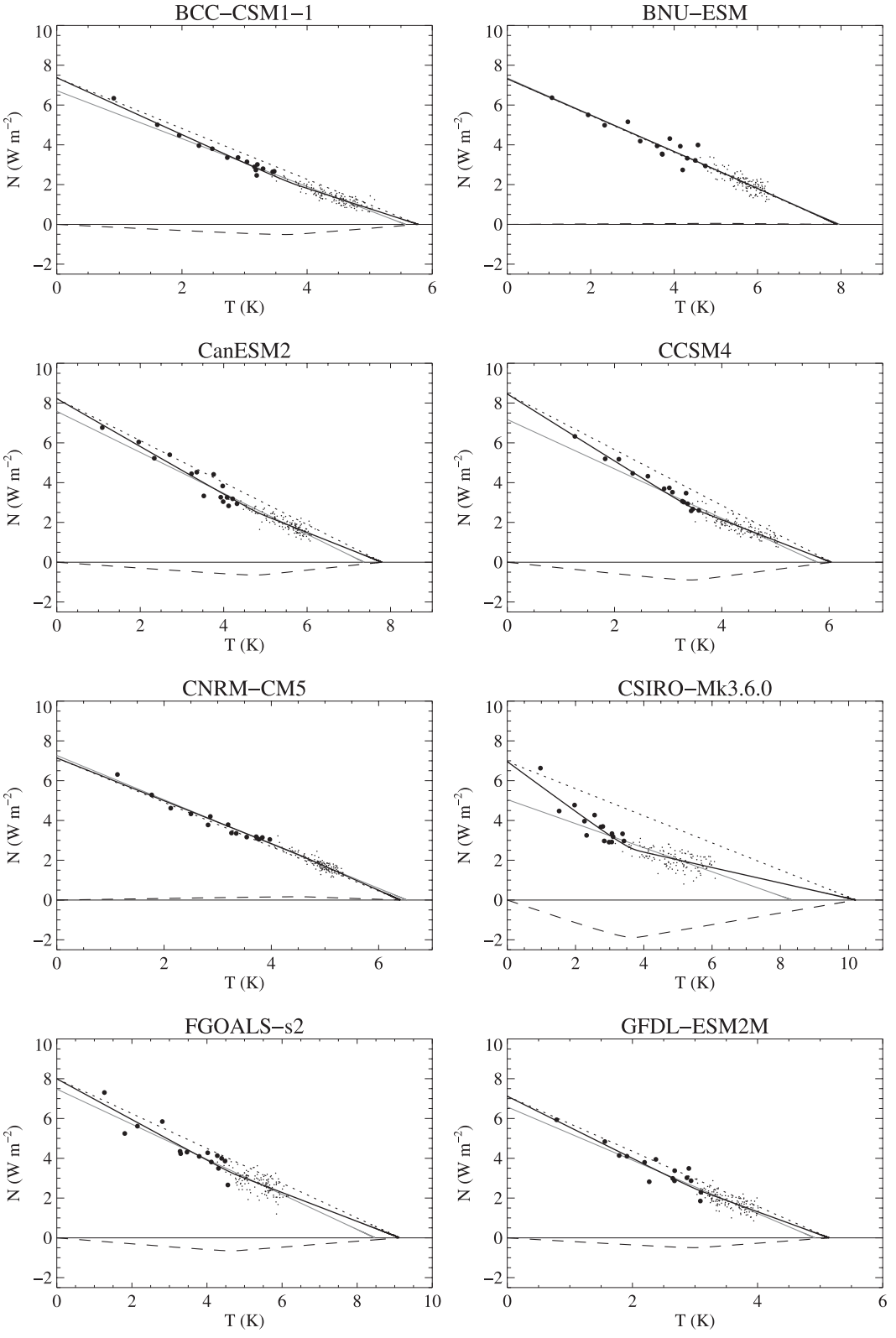

FIG. 2. Global annual mean net radiative flux change at TOA N as a function of global mean surface air temperature response T for the abrupt $4\times CO_2$ experiments (black dots; large dots for the first 15 yr), for the 16 AOGCMs. The thick black line is the EBM-ε fit. The dotted and dashed black lines show the linear contribution $\mathcal{F} - \lambda T$ and the deviation contribution $-(\varepsilon - 1)H$, respectively. The gray line is the linear fit of Gregory et al. (2004). The thin black line shows $N = 0$. Note that the range of T can differ from one panel to another.

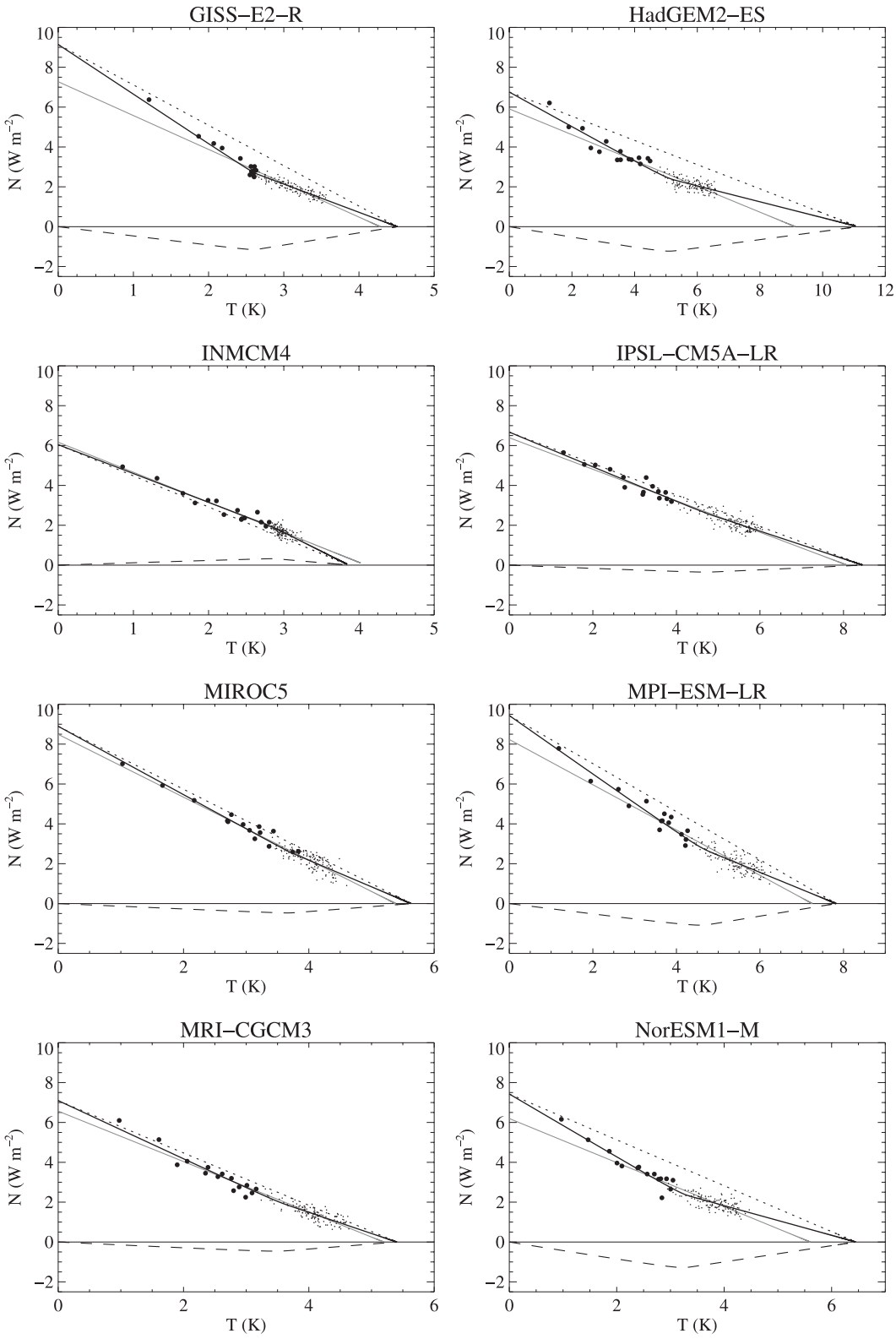

FIG. 2. (*Continued*)

CMIP3 model's analysis despite methodological differences. Winton et al. (2010) derived the value of ε from 1% yr^{-1} CO_2 increase experiments using equilibrium climate sensitivity mainly derived from AGCMs coupled with a mixed-layer ocean model and using forcing estimates taken from Solomon et al. (2007). The latter were computed from different sources and they took into account either only the stratospheric adjustment or both stratospheric and tropospheric adjustments [through the method of Gregory et al. (2004)], depending on cases. In this study, the efficacy factor ε, the radiative forcing, and the equilibrium climate sensitivity are derived jointly in the single framework of the EBM-ε.

Figure 2 compares for each model the N–T plot for AOGCM results, EBM-ε fit, and the linear regression of Gregory et al. (2004). For models with an efficacy factor near 1 (BNU-ESM, CNRM-CM5.1, and IPSL-CM5A-LR), the assumption of linearity between N and T is valid and the results from EBM-ε are close to that of the linear model. For models with a large ε (CSIRO-Mk3.6.0, GISS-E2-R, HadGEM2-ES, MPI-ESM-LR, and NorESM1-M), the results from EBM-ε largely improve the fit of radiative imbalance versus temperature response compared to a linear fit. In particular, the EBM-ε is able to reproduce the two-stage behavior of these models in the parameter space (N, T).

Figures 3b–d compare the values of the $4\times CO_2$ radiative forcing $\mathcal{F}_{4\times CO_2}$, λ, and the $4\times CO_2$ equilibrium temperature response $T_{4\times CO_2}$ obtained within the framework of the EBM-ε and those derived with the method described in Gregory et al. (2004). The three AOGCMs with ε larger than 1.5 are indicated with filled red square, circle, and triangle symbols. For these models, the radiative forcing amplitude and the equilibrium climate sensitivity are larger than in the standard linear model estimate. Indeed, for CSIRO-Mk3.6.0 and HadGEM2-ES, the equilibrium temperature response for a $4\times CO_2$ perturbation is up to 2 K warmer than the value derived from the linear assumption. The multimodel mean is 0.5 K warmer. The radiative forcing is 1–2 W m^{-2} larger for large ε models and the multimodel mean is 0.7 W m^{-2} larger. Most models have a forcing lower than 8.5 W m^{-2} except CCSM4, GISS-E2-R, MPI-ESM-LR, and MIROC5. The three latter have a forcing on the order of 9 W m^{-2}, which suggests a strong effect of the tropospheric adjustment. The change in the ECS is mainly due to a change in the forcing with the radiative feedback parameters being less impacted (except for the GISS-E2-R model). Moreover, unlike the forcing and the equilibrium temperature, the sign of the difference in λ between the EBM-1 and the EBM-ε estimates is independent of the sign of ε-1. For example, for HadGEM2-ES and CSIRO-Mk3.6.0, λ is larger and smaller in the EBM-ε framework than in the EBM-1 framework, respectively, whereas both have an ε value greater than 1. The multimodel radiative forcing and radiative feedback parameter standard deviations are roughly unchanged whereas that of the equilibrium temperature increases from 1.6 to 2.1 K. The improved match of the temperature response and radiative imbalance evolution between the AOGCMs and the simple EBM suggests that the values estimated from the EBM-ε method are more accurate. However, a complete assessment of the EBM-ε would require to extend AOGCM experiments until equilibrium (i.e., over a period of 1000–1500 years). Indeed, the strength of the feedbacks can saturate, which would impact the equilibrium temperature response (Li et al. 2013).

b. *Thermal inertia parameters and temperature: Comparison with the EBM-1*

The thermal inertia physical parameters and the relaxation times are given in Table 2 and represented as a function of their EBM-1 counterparts in Figs. 3e–i. The fast relaxation time scale τ_f is not impacted by the inclusion of the efficacy of deep-ocean heat uptake, whereas the slow relaxation time scale τ_s is. The change in τ_s is mainly due to change in the heat-exchange coefficient γ rather than in the deep-ocean heat capacity C_0. Models with $\varepsilon > 1$ have a lower γ than in the EBM-1 framework. The inclusion of the effect represented by the deviation term $(1 - \varepsilon)H$ in the temperature response amounts to modifying the deep-ocean heat uptake such that the heat-exchange coefficient is $\varepsilon\gamma$. The lack of efficacy factor in the EBM-1 is compensated by a large γ for models with $\varepsilon > 1$ in the EBM-ε framework.

The EBM-1 also underestimates the upper-ocean heat capacity C. The estimate of C depends on the forcing estimation since it is evaluated through an estimation of the temperature tendency at $t = 0$ that is equal to $\mathcal{F}/C$. Consequently, an underestimation of $\mathcal{F}$ leads to an underestimation of C. These results suggest that the lack of radiative effect associated with deep-ocean heat uptake introduces a bias in the EBM-1 estimates of the thermal inertia parameters. The standard deviations of γ, C_0, and C are reduced with the EBM-ε from 0.18 to 0.15 W m^{-2} K^{-1}, 62 to 52 W yr m^{-2} K^{-1} (but slightly increased from 27 to 29 W yr m^{-2} K^{-1} if INM-CM4 is excluded), and 1.1 to 0.9 W yr m^{-2} K^{-1}, respectively. This shows that introducing a new degree of freedom reduces slightly the intermodel spread.

Figure 4 shows the temperature response of the three AOGCMs with the largest ε estimates (CSIRO-Mk3.6.0, NorESM1-M, and HadGEM2-ES) for the abrupt $4\times CO_2$ and the 1% yr^{-1} CO_2 experiments, as well as the EBM-1 and the EBM-ε analytical solutions using the parameters

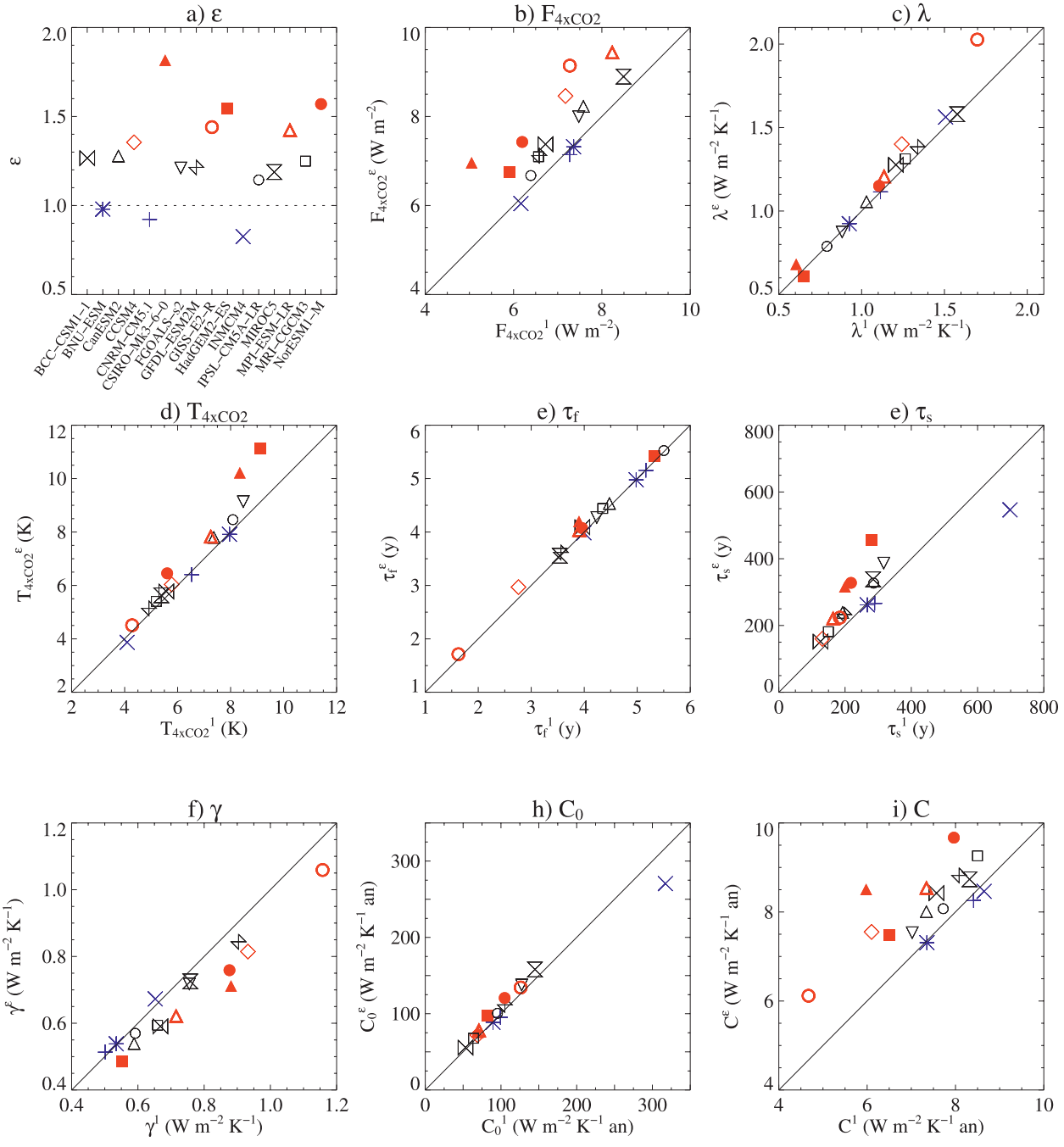

FIG. 3. Parameter estimates of (a) ε values for the 16 AOGCMs and (b) EBM-ε estimates as a function of EBM-1 estimates for $\mathcal{F}_{4\times CO_2}$, (c) λ, (d) $T_{4\times CO_2}$, (e) τ_f, (f) τ_s, (g) γ, (h) C_0, and (i) C. Superscripts 1 and ε denote estimates from the EBM-1 and the EBM-ε methods, respectively. The dotted line shows $\varepsilon = 1$ in (a) and the solid lines indicate a perfect match between EBM-ε and EBM-1 estimates in (b)–(i). Each symbol corresponds to one AOGCM.

estimated by the corresponding method on the basis of the abrupt $4\times CO_2$ experiment. The temperature responses are identical for both EBMs in both the abrupt $4\times CO_2$ and the 1% yr^{-1} CO_2 simulations over the first 150 years, and they match the AOGCM responses. But, for the step-forcing scenario, the EBM-ε response diverges from the EBM-1 response after about 300 years. Only the second phase of the temperature evolution, the one driven by the slow component of the system, is modified by the introduction of an efficacy factor. This is consistent with the fact that only the slow relaxation time scale varies between the EBM-1 and the

TABLE 2. The atmosphere/land/upper-ocean heat capacity C, deep-ocean heat capacity C_0, heat-exchange coefficient γ, and fast and slow relaxation times estimates in the framework of the EBM-ε of the 16 CMIP5 models used in this paper, and their multimodel mean and standard deviation.

Model	C (W yr m^{-2} K^{-1})	C_0 (W yr m^{-2} K^{-1})	γ (W m^{-2} K^{-1})	τ_f (yr)	τ_s (yr)
BCC-CSM1–1	8.4	56	0.59	4.1	152
BNU-ESM	7.3	89	0.54	5.0	262
CanESM2	8.0	77	0.54	4.5	239
CCSM4	7.6	72	0.81	3.0	160
CNRM-CM5.1	8.3	95	0.51	5.2	266
CSIRO-Mk3.6.0	8.5	76	0.71	4.2	316
FGOALS-s2	7.5	138	0.72	4.3	387
GFDL-ESM2M	8.8	112	0.84	3.6	233
GISS-E2-R	6.1	134	1.06	1.7	224
HadGEM2-ES	7.5	98	0.49	5.4	457
INM-CM4	8.5	271	0.67	4.0	546
IPSL-CM5A-LR	8.1	100	0.57	5.5	327
MIROC5	8.7	158	0.73	3.6	338
MPI-ESM-LR	8.5	78	0.62	4.0	220
MRI-CGCM3	9.3	68	0.59	4.4	181
NorESM1-M	9.7	121	0.76	4.1	328
Multimodel mean	8.2	109	0.67	4.2	290
Standard deviation	0.9	52	0.15	0.9	107

EBM-ε methods. The EBM-1 calibrated with the abrupt simulation is accurate enough to represent the temperature evolution over the centennial scale. However, compared to the EBM-ε estimates, the EBM-1 parameters are biased as a result of a bias in radiative parameters estimated following the method of Gregory et al. (2004).

c. Parameter dependency

In this section, the question of potential relationships between the EBM-ε parameters is investigated. Table 3 shows the multimodel correlations between parameters of the EBM-ε, and also between these parameters and the equilibrium temperature response. For the set of 16 models, a correlation coefficient higher than 0.50 is significant at the 95% confidence level (two-tailed test). Note that the statistical test assumes that the AOGCMs are independent. As expected, the anticorrelation between T_{eq} and λ is high, with a correlation coefficient of -0.84. No correlation is found between $\mathcal{F}$ and λ, suggesting that the effect of fast tropospheric adjustment is independent of the surface temperature feedback. Consistently, the equilibrium temperature is independent of the adjusted forcing magnitude.

Raper et al. (2002) suggested a negative correlation between their heat-exchange coefficient κ of the one-layer model (that is similar to the parameter γ) and the radiative feedback parameter λ but the analysis of CMIP3 models by Gregory and Forster (2008) and Plattner et al. (2008) did not find such a correlation. Including an interactive deep ocean changes the formulation of deep-ocean heat uptake and impacts the

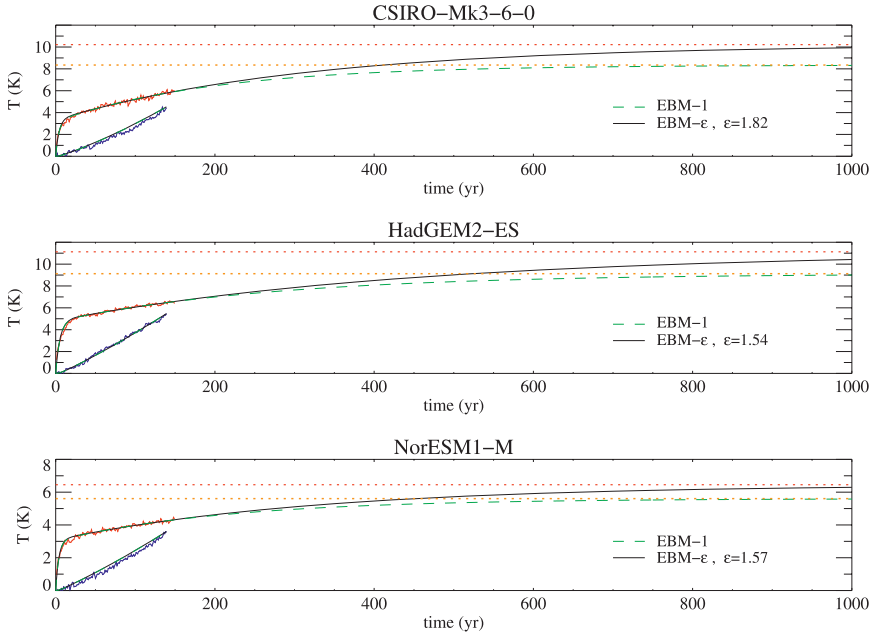

FIG. 4. Temperature response of AOGCMs with the highest ε value for the abrupt $4\times CO_2$ (red lines) and 1% yr^{-1} CO_2 (blue lines) experiments and corresponding fit for EBM-1 (dashed green) and EBM-ε (solid black). Note that the EBM-1 and the EBM-ε solutions are superposed for the 1% yr^{-1} CO_2 and the beginning of the abrupt $4\times CO_2$ experiments. The dotted lines denote the equilibrium temperature for EBM-1 (orange) and EBM-ε (red).

TABLE 3. Multimodel correlations between the equilibrium temperature at 4×CO_2 $T_{4\times CO_2}$ and the physical parameters F, λ, ε, γ, C_0, and C of the EBM-ε for the 16 CMIP5 AOGCMs. Boldface correlations are significant at the 95% confidence level.

	$T_{4\times CO_2}$	$\mathcal{F}$	λ	ε	γ	C_0	C
$T_{4\times CO_2}$	1	−0.11	**−0.84**	0.44	−0.45	−0.38	−0.14
$\mathcal{F}$		1	0.41	0.24	0.40	−0.21	−0.28
λ			1	−0.22	**0.64**	0.36	−0.11
ε				1	0.26	−0.42	0.04
γ					1	0.24	−0.24
C_0						1	−0.01
C							1

relationship between the heat-exchange coefficient (κ or γ) and the radiative feedback parameter λ. Indeed, the EBM-ε estimates of λ and γ are positively correlated, contrary to the results of Raper et al. (2002), with a correlation coefficient of 0.64. This value is above the significant level. However, excluding the GISS-E2-R model, which is largely outside the range of the model ensemble, the correlation is not significant with a value of 0.43, showing the limited robustness of this correlation. The remaining interparameter correlations are found to not be significant.

d. Decomposition in longwave and shortwave contributions

In this section, the net TOA radiative flux is decomposed into longwave (LW) and shortwave (SW) components N^{LW} and N^{SW}, respectively. The net radiative imbalance N is the right-hand side of Eq. (15). It can be expressed as follows [from Eqs. (12) and (16)]:

$$N = \mathcal{F} - \lambda T - (\lambda - \lambda_D)\frac{\varepsilon}{\lambda}H. \tag{30}$$

We introduce LW and SW radiative feedback parameters associated with the deep-ocean heat-uptake temperature, λ_D^{LW} and λ_D^{SW}, and we assume the decomposition in an upper-ocean and a deep-ocean radiative contribution is valid for each component separately. These assumptions yield the following equations:

$$N^{LW} = \mathcal{F}^{LW} - \lambda^{LW}T - (\lambda^{LW} - \lambda_D^{LW})\frac{\varepsilon}{\lambda}H \quad \text{and} \tag{31}$$

$$N^{SW} = \mathcal{F}^{SW} - \lambda^{SW}T - (\lambda^{SW} - \lambda_D^{SW})\frac{\varepsilon}{\lambda}H, \tag{32}$$

where $\mathcal{F}^{LW}$, $\mathcal{F}^{SW}$, λ^{LW}, and λ^{SW} are the LW and SW components of the radiative forcing and of the radiative feedback parameter, respectively. Unlike in the case of the total feedback, we do not define an SW or LW efficacy factor ε_{SW} or ε_{LW}. Indeed, although the total feedback is necessarily different from zero, it is possible that λ^{SW} (λ_D^{SW}) is zero while λ_D^{SW} (λ^{SW}) is not. In such a case, a shortwave efficacy factor ε_{SW} would make no sense.

Each LW and SW component is calculated by multilinear regression of the corresponding net radiation flux as a function of temperature (both from the AOGCM abrupt 4×CO_2 experiment) and $(\varepsilon/\lambda)H$ (from the EBM-ε estimation). Values of the tuned LW and SW radiative parameters are reported in Table 4 and resulting fits for each model separately shown in Fig. 5. These figures reflect the large intermodel spread in both forcing and radiative feedback parameters LW and SW components.

TABLE 4. The LW and SW components of the radiative forcing, $\mathcal{F}^{LW}$ and $\mathcal{F}^{SW}$, of the total feedback parameter, λ^{LW} and λ^{SW}, and of the deep-ocean heat-uptake feedback parameter, λ_D^{LW} and λ_D^{SW}, estimates in the framework of the EBM-ε of the 16 CMIP5 models used in this paper, and their multimodel mean and standard deviation.

Model	$\mathcal{F}^{LW}$ (W m^{-2})	$\mathcal{F}^{SW}$ (W m^{-2})	λ^{LW} (W m^{-2} K^{-1})	λ^{SW} (W m^{-2} K^{-1})	λ_D^{LW} (W m^{-2} K^{-1})	λ_D^{SW} (W m^{-2} K^{-1})
BCC-CSM1–1	6.4	1.0	1.69	−0.42	1.68	−0.68
BNU-ESM	6.6	0.7	1.57	−0.65	1.50	−0.56
CanESM2	6.2	2.0	1.42	−0.37	1.38	−0.56
CCSM4	7.1	1.4	1.94	−0.54	1.82	−0.79
CNRM-CM5.1	5.1	2.1	1.62	−0.50	1.67	−0.46
CSIRO-Mk3.6.0	7.4	−0.4	1.97	−1.29	1.81	−1.43
FGOALS-s2	8.7	−0.7	1.34	−0.47	1.28	−0.56
GFDL-ESM2M	5.4	1.7	1.37	0.01	1.68	−0.54
GISS-E2-R	7.7	1.5	1.48	0.55	1.25	0.16
HadGEM2-ES	6.2	0.6	1.56	−0.96	1.55	−1.16
INM-CM4	6.8	−0.7	2.12	−0.55	2.65	−0.76
IPSL-CM5A-LR	3.4	3.3	1.92	−1.13	1.89	−1.20
MIROC5	6.9	2.0	1.93	−0.35	1.70	−0.37
MPI-ESM-LR	7.0	2.5	1.67	−0.46	1.50	−0.65
MRI-CGCM3	6.6	0.5	2.24	−0.93	2.16	−1.11
NorESM1-M	6.3	1.1	1.82	−0.67	1.67	−0.93
Mean	6.5	1.2	1.73	−0.54	1.70	−0.72
Standard deviation	1.2	1.1	0.27	0.44	0.34	0.38

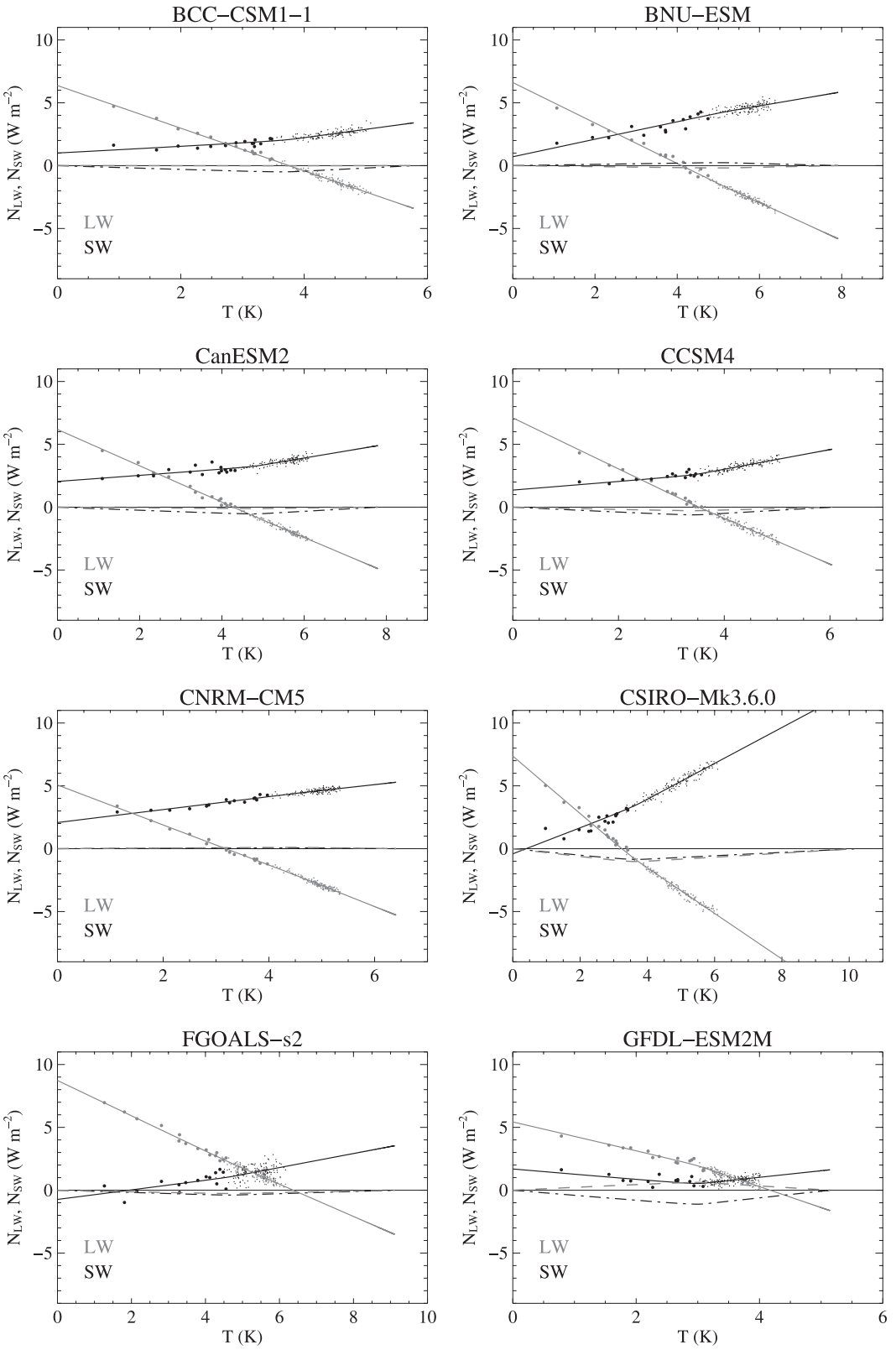

FIG. 5. Global annual mean net LW (gray) and SW (black) radiative flux change at TOA as a function of global mean surface air temperature response T for the abrupt $4\times CO_2$ experiments (black dots; large dots for the first 15 years), for the 16 AOGCMs. The thick gray and black lines are the EBM-ε fits of the LW and the SW radiative flux, respectively. The dashed gray lines and the dot-dashed black lines show the LW and SW components of the $-(\varepsilon - 1)H$ term, respectively. The thin black line shows $N = 0$. Note that the range of T can differ from one panel to another.

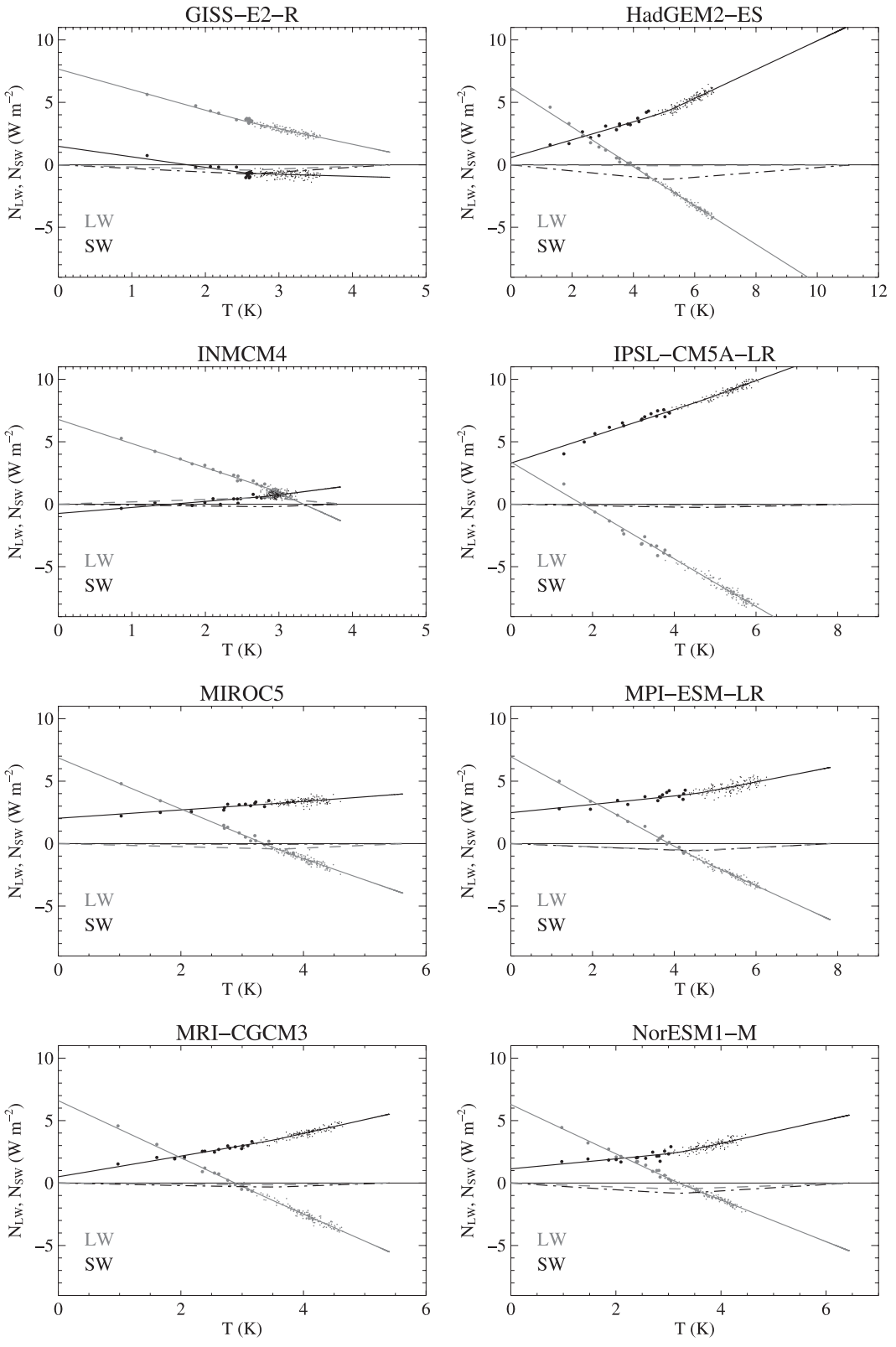

FIG. 5. (*Continued*)

AOGCMs that have a large SW forcing contribution can have a large LW contribution (MPI-ESM-LR) or a small LW contribution (IPSL-CM5A-LR). The $4\times CO_2$ LW forcing ranges from 3.4 to 8.7 W m^{-2} with an ensemble mean of 6.5 W m^{-2} and a standard deviation of 1.2 W m^{-2}. Except for three models (CSIRO-Mk3.6.0, FGOALS-s2, INM-CM4), the $4\times CO_2$ SW forcing is mostly positive with a mean value of 1.2 W m^{-2}. Its standard deviation (1.1 W m^{-2}) is on the same order as that of the LW contribution. By comparison with estimates taking into account the stratospheric adjustment only, the forcing is found to be lower in the LW and larger in the SW. Indeed, Forster and Taylor (2006) found a forcing estimate of 3.45 W m^{-2} in the LW for a $2\times CO_2$ experiment (corresponding to 6.90 W m^{-2} for a $4\times CO_2$ experiment). The instantaneous SW forcing is on the order of -0.06 W m^{-2} (Myhre et al. 1998). These estimates confirm Gregory and Webb (2008) and suggest a nonnegligible effect of the fast change in the cloud component (among the other feedbacks) on the radiative forcing adjustment.

The LW contribution λ^{LW} to the feedback parameter is positive (i.e., negative feedback) for all models because the radiative imbalance is restored by increased LW emission associated with the temperature increase. The SW contribution to the feedback parameter λ^{SW} is negative (i.e., positive feedback) for all models except GFDL-ESM2M, which has a negligible λ^{SW}, and GISS-E2-R. For most AOGCMs, λ^{SW} is above (in absolute value) the 0.2–0.4 W m^{-2} K^{-1} typical range of the albedo feedback, suggesting a positive feedback of clouds in the SW.

The deep-ocean heat-uptake feedback parameter λ_D^{LW} is generally of the same order of magnitude as λ^{LW} but λ_D^{SW} is smaller than λ^{SW}. This suggests that the value of $\varepsilon > 1$ obtained for the majority of the models is mainly due to the shortwave radiation, with low clouds as a good candidate to explain most of the difference between EBM-ε and EBM-1. Further analysis is necessary to understand which components of the climate system are responsible for the differences and to quantify each contribution. But the results of such a simple SW/LW decomposition suggest that the EBM-ε framework can be used to decompose the radiative fluxes such as a cloud/clear-sky decomposition or more complex decompositions such as partial radiative fluxes.

4. Conclusions

In this study, the two-layer energy-balance model with an efficacy factor of deep-ocean heat uptake is used as a tool to estimate the first-order global thermal properties of AOGCMs. These thermal properties include both radiative properties and thermal inertia properties. It is shown that the temperature response can be decomposed as the balanced response to three "forcings": the TOA radiative forcing, the upper-ocean heat uptake, and the deep-ocean heat uptake. Assuming additivity of each temperature response pattern to these forcings and assuming the separability of time and spatial variability of these temperature responses, the radiative feedback parameter associated with the deep-ocean heat uptake is shown to be different from the equilibrium feedback parameter, since the local feedback parameter varies geographically. This results in the presence of an additional term in the radiative imbalance formulation depending on the deep-ocean heat uptake.

Within this EBM-ε framework, the concepts of effective forcing and effective climate sensitivity are unchanged but the concept of an effective feedback parameter is modified. The effective forcing remains the physical parameter defined by Gregory et al. (2004); that is, the value of the net radiative imbalance when the temperature tends to zero. It is sensitive to fast feedbacks due to changes in both stratospheric and tropospheric variables, such as clouds, temperature lapse rate, and water vapor amount, associated with the external radiative perturbation, but unrelated to the surface temperature response. However, the effective climate feedback parameter as usually defined (i.e., the feedback parameter of the transient regime) needs to be distinguished from the equilibrium feedback parameter. The effective equilibrium feedback parameter is assumed to be constant for a given type of forcing agent and a given spatial distribution of the forcing amplitude but it is only valid for an equilibrium state. The transient feedback factor involves an additional term that can depend on deep-ocean heat uptake and it can thus vary in time.

An iterative method of calibration is proposed and applied to 16 CMIP5 AOGCMs. The results show that the model reproduces with accuracy the evolution of the radiative imbalance as a function of the temperature response during a transient regime. The fits of the temperature evolution over the time of simulation ($\sim$150 yr) are the same as those obtained with the EBM-1. However, the physical parameters of the model are different. The improved match of the temperature response and radiative imbalance evolution between the AOGCMs and the EBM suggests that the values estimated from the EBM-ε method are more accurate. Moreover, the method is applied to the LW and the SW components of the radiative flux. Each evolution separately is well represented, suggesting that the method can be applied to a partial decomposition of the radiative imbalance.

The benefit of two-layer EBMs such as the EBM-1 and EBM-ε is that they are the simplest EBMs that represent both the beginning of the simulation (determined by the forcing) and the end of the experiment (determined by the equilibrium climate sensitivity for a constant forcing). One-layer EBMs are unable to represent both phases of the time evolution. At short time scales, the advantage of the EBM-ε over the EBM-1 is that the net TOA imbalance is better represented as a function of the global surface temperature response. The EBM-ε can be used to compute the radiative parameters and the effective climate sensitivity consistently from one single methodology and one single short AOGCM experiment, by taking into account the time variation of the effective feedback factor. From this point of view, the calibration of the EBM-ε method constitutes a new, improved method to determine the climate sensitivity and the adjusted forcing of an AOGCM. However, the use of a two-layer EBM can be limited in representing long time experiments because other time scales can emerge above 150 years.

Such a two-layer EBM offers a complete first-order explanation of the behavior of climate models under an externally imposed perturbation. The spread on the radiative and thermal inertia global parameters within a generation of models (such as the CMIP5 generation) can be used as an indication of the uncertainty of the multimodel climate projections performed for the Intergovernmental Panel on Climate Change (IPCC). The evolution of this spread from one CMIP exercise to the next indicates whether AOGCMs converge in terms of global properties. It can also be used for analysis of AOGCMs, by relating some of the EBM parameters to physical processes or physical variables that can be directly calculated in the AOGCM. In parallel, the calibration of such a model, which could be extended to other types of radiative perturbations, offers a physically based simple climate model able to emulate the AOGCM response to different idealized scenarios.

Acknowledgments. We gratefully thank Jonathan Gregory for his careful and constructive review of the paper and two anonymous reviewers for their comments that helped to improve the manuscript. We thank Julien Boé, Aurélien Ribes, and Laurent Terray for helpful discussions and valuable comments on the work. Thanks are also due to Isaac Held for sharing interesting ideas in his blog. This work was supported by the European Union FP7 Integrated Project COMBINE. We acknowledge the World Climate Research Programme's Working Group on Coupled Modelling, which is responsible for CMIP, and the U.S. Department of Energy's Program for Climate Model Diagnosis and Intercomparison which provides coordinating support and led development of software infrastructure in partnership with the Global Organization for Earth System Science Portals. We thank the climate modeling groups for producing and making available their model output.

REFERENCES

Andrews, T., J. M. Gregory, M. J. Webb, and K. E. Taylor, 2012: Forcing, feedbacks and climate sensitivity in CMIP5 coupled atmosphere–ocean climate models. *Geophys. Res. Lett.,* **39,** L09712, doi:10.1029/2012GL051607.

Boer, G., and B. Yu, 2003a: Climate sensitivity and response. *Climate Dyn.,* **20,** 415–429.

——, and ——, 2003b: Climate sensitivity and climate state. *Climate Dyn.,* **21,** 167–176.

Forster, P. M., and K. E. Taylor, 2006: Climate forcings and climate sensitivities diagnosed from coupled climate model integrations. *J. Climate,* **19,** 6181–6194.

——, M. Blackburn, R. Glover, and K. P. Shine, 2000: An examination of climate sensitivity for idealised climate change experiments in an intermediate general circulation model. *Climate Dyn.,* **16,** 833–849.

Geoffroy, O., D. Saint-Martin, D. J. L. Olivié, A. Voldoire, G. Bellon, and S. Tytéca, 2013: Transient climate response in a two-layer energy-balance model. Part I: Analytical solution and parameter calibration using CMIP5 AOGCM experiments. *J. Climate,* **26,** 1841–1857.

Gregory, J. M., and P. M. Forster, 2008: Transient climate response estimated from radiative forcing and observed temperature change. *J. Geophys. Res.,* **113,** D23105, doi:10.1029/2008JD010405.

——, and M. Webb, 2008: Tropospheric adjustment induces a cloud component in CO_2 forcing. *J. Climate,* **21,** 58–71.

——, and Coauthors, 2004: A new method for diagnosing radiative forcing and climate sensitivity. *Geophys. Res. Lett.,* **31,** L03205, doi:10.1029/2003GL018747.

Hansen, J., and Coauthors, 2005: Efficacy of climate forcings. *J. Geophys. Res.,* **110,** D18104, doi:10.1029/2005JD005776.

Held, I. M., M. Winton, K. Takahashi, T. Delworth, F. Zeng, and G. K. Vallis, 2010: Probing the fast and slow components of global warming by returning abruptly to preindustrial forcing. *J. Climate,* **23,** 2418–2427.

Knutti, R., and G. C. Hegerl, 2008: The equilibrium sensitivity of the Earth's temperature to radiation changes. *Nat. Geosci.,* **1,** 735–743.

Li, C., J.-S. von Storch, and J. Marotzke, 2013: Deep-ocean heat uptake and equilibrium climate response. *Climate Dyn.,* doi:10.1007/s00382-012-1350-z, in press.

Manabe, S., R. J. Stouffer, M. J. Spelman, and K. Bryan, 1991: Transient responses of a coupled ocean–atmosphere model to gradual changes of atmospheric CO_2. Part I: Annual mean response. *J. Climate,* **4,** 785–818.

Murphy, J. M., 1995: Transient response of the Hadley Centre coupled ocean–atmosphere model to increasing carbon dioxide. Part III: Analysis of global-mean response using simple models. *J. Climate,* **8,** 496–514.

Myhre, G., E. Highwood, K. Shine, and F. Stordal, 1998: New estimates of radiative forcing due to well mixed greenhouse gases. *Geophys. Res. Lett.,* **25,** 2715–2718.

Plattner, G.-K., and Coauthors, 2008: Long-term climate commitments projected with climate–carbon cycle models. *J. Climate,* **21,** 2721–2751.

Raper, S. C. B., J. M. Gregory, and R. J. Stouffer, 2002: The role of climate sensitivity and ocean heat uptake on AOGCM transient temperature response. *J. Climate,* **15,** 124–130.

Senior, C. A., and J. F. B. Mitchell, 2000: The time-dependence of climate sensitivity. *Geophys. Res. Lett.,* **27,** 2685–2688.

Solomon, S., D. Qin, M. Manning, M. Marquis, K. B. Averyt, M. Tignor, H. L. Miller, and Z. Chen, Eds., 2007: *Climate Change 2007: The Physical Science Basis.* Cambridge University Press, 996 pp.

Williams, K. D., W. J. Ingram, and J. M. Gregory, 2008: Time variation of effective climate sensitivity in GCMs. *J. Climate,* **21,** 5076–5090.

Winton, M., K. Takahashi, and I. M. Held, 2010: Importance of ocean heat uptake efficacy to transient climate change. *J. Climate,* **23,** 2333–2344.